Published in final edited form as:

Nat Nanotechnol. 2017 September ; 12(9): 877–882. doi:10.1038/nnano.2017.113.

Antigen-capturing nanoparticles improve the abscopal effect and cancer immunotherapy

Yuanzeng Min[1,2,3], **Kyle C. Roche**[1,2,3], **Shaomin Tian**[2,4], **Michael J. Eblan**[1,2,3], **Karen P. McKinnon**[2,4], **Joseph M. Caster**[1,2,3], **Shengjie Chai**[2,5], **Laura E. Herring**[6], **Longzhen Zhang**[7], **Tian Zhang**[8], **Joseph M. DeSimone**[2,4,9,10,11,12], **Joel E. Tepper**[1,2,3], **Benjamin G. Vincent**[2,5], **Jonathan S. Serody**[2,4,5], and **Andrew Z. Wang**[1,2,3,7,*]

[1]Laboratory of Nano- and Translational Medicine, Carolina Center for Cancer Nanotechnology Excellence, Carolina Institute of Nanomedicine, University of North Carolina at Chapel Hill, Chapel Hill, North Carolina 27599, United States

[2]Lineberger Comprehensive Cancer Center, University of North Carolina at Chapel Hill, Chapel Hill, North Carolina 27599, United States

[3]Department of Radiation Oncology, University of North Carolina at Chapel Hill, Chapel Hill, North Carolina 27599, United States

[4]Department of Microbiology & Immunology, University of North Carolina at Chapel Hill, Chapel Hill, North Carolina 27599, United States

[5]Department of Medicine, University of North Carolina at Chapel Hill, Chapel Hill, North Carolina 27599, United States

[6]UNC Proteomics Core Facility, Department of Pharmacology, University of North Carolina, Chapel Hill, NC, USA, 27599

[7]Jiangsu Center for the Collaboration and Innovation of Cancer Biotherapy, Cancer Institute, Xuzhou Medical University, Xuzhou, Jiangsu, China

[8]Division of Medical Oncology, Department of Medicine, Duke University Medical Center, Durham, North Carolina 27710, United States

[9]Division of Molecular Pharmaceutics, Eshelman School of Pharmacy, University of North Carolina, Chapel Hill, NC 27599, USA

*Corresponding author: zawang@med.unc.edu.
Correspondence and requests for materials should be addressed to A.W.

Author contributions

A.Z.W. and T.Z. conceived and designed the experiments with Y.M and K.C.R. Y.M. and M.J.E. performed the efficacy study. Y.M. also performed the mechanistic study with S.T.'s and K.M.'s help. L.H. processed all raw mass spectrometry data. S.C. and B.G.V. analyzed mass spectrometry data for neoantigens. All authors analyzed and discussed the data. A.Z.W., Y.M. and K.C.R. wrote the manuscript.

Supplementary information is available in the online version of the paper.

Publisher's note: Springer Nature remains neutral with regard to jurisdictional claims in published maps and institutional affiliations.

Competing financial interests

The authors declare no competing financial interests.

[10]Department of Chemistry, University of North Carolina, Chapel Hill, NC 27599, USA

[11]Department of Chemical and Biomolecular Engineering, NC State University, Raleigh, NC 27695, USA

[12]Sloan-Kettering Institute for Cancer Research, Memorial Sloan-Kettering Cancer Center, New York, NY 10021, USA

Abstract

Immunotherapy holds tremendous promise for improving cancer treatment[1]. Administering radiotherapy with immunotherapy has been shown to improve immune responses and can elicit an "abscopal effect"[2]. Unfortunately, response rates for this strategy remain low[3]. Herein, we report an improved cancer immunotherapy approach that utilizes antigen-capturing nanoparticles (AC-NPs). We engineered several AC-NPs formulations and demonstrated that the set of protein antigens captured by each AC-NP formulation is dependent upon NP surface properties. We showed that AC-NPs deliver tumor specific proteins to antigen-presenting cells and significantly improve the efficacy of αPD-1 treatment using the B16F10 melanoma model, generating up to 20% cure rate as compared to 0% without AC-NPs. Mechanistic studies revealed that AC-NPs induced an expansion of $CD8^+$ cytotoxic T cells and increased both $CD4^+/T_{reg}$ and $CD8^+/T_{reg}$ ratios. Our work presents a novel strategy for improving cancer immunotherapy with nanotechnology.

Cancer immunotherapy has emerged as a powerful new strategy in cancer treatment[4]. Antibodies that block negative immune regulatory pathways (checkpoint inhibitors)[5], including CTLA-4 (cytotoxic T-lymphocyte–associated antigen 4) and PD-1 (programmed cell death 1) receptors, improve survival in patients with advanced disease such as melanoma, bladder, squamous cell head and neck and non-small-cell lung cancer[6–11]. A key clinical approach to improving cancer immunotherapy has been to combine radiotherapy with checkpoint inhibitors to induce the abscopal effect, a phenomenon where local tumor treatment produces systemic regression of metastatic lesions[12]. The abscopal effect is facilitated by the immune system and has been found anecdotally to mediate long-term, durable clinical responses. The synergistic interaction between radiotherapy and immunotherapy is thought to be due to immune stimulation by radiation-induced pro-inflammatory protein production and increased exposure of immune cells to cancer specific antigens that are released following radiotherapy-induced cancer cell death[13–16]. We hypothesized that NPs could be used to improve treatment response to immunotherapy and to induce the abscopal effect by capturing tumor-derived protein antigens (TDPA) released during radiotherapy and transporting them to antigen presenting cells (APCs), thereby promoting cancer immunity (Figure 1)[17–22].

As proof of concept, herein we report on the development and use of several antigen-capturing nanoparticles (AC-NP) formulations to improve cancer immunotherapy. NPs were formulated using poly (lactic-co-glycolic acid) (PLGA), a biocompatible and biodegradable polymer. The NPs' surfaces were modified to enable binding of TDPAs by a variety of mechanisms. Unmodified PLGA AC-NPs bind to proteins through non-covalent hydrophobic-hydrophobic interactions. AC-NPs coated with amine- polyethylene glycol

(NH_2-PEG) (NH_2 AC-NP) and 1,2-Dioleoyloxy-3-(trimethylammonium)propane (DOTAP AC-NP) both bind to proteins via ionic interactions. AC-NPs coated with maleimide-PEG (Mal AC-NP) bind to proteins by forming stable thioether bonds. As a negative control, we also formulated AC-NPs with methoxy-PEG (mPEG), which should have minimal interactions with proteins[23].

We first sought to determine whether the surface chemistry of AC-NPs impacted TDPA capture. AC-NPs were incubated with lethally irradiated B16F10 melanoma cell lysates *ex vivo*. Both the size and zeta potential of AC-NPs changed following incubation (Supplementary Figure 1a, b), indicating successful TDPA capture by AC-NPs. Successful TDPA capture was confirmed by quantifying the total amount of protein bound by each AC-NP formulation. mPEG AC-NPs captured very little protein, a finding consistent with its anti-biofouling surface. All other AC-NP formulations captured relatively high amounts of protein (Supplementary Figure 1c). AC-NP bound proteins were then isolated and identified using mass spectrometry. We found that the diversity and composition of proteins captured by AC-NPs is dependent upon their surface chemistries. The PLGA and DOTAP AC-NP formulations captured the most comprehensive set of proteins (Figure 2a). Additionally, while some proteins were captured by multiple AC-NP formulations, some were discretely captured by only one AC-NP formulation (Figure 2b).

To determine whether AC-NPs captured tumor-specific antigens, we performed an *in silico* analysis on our mass spectrometry data to determine if any of the captured proteins contain neoantigens expressed by B16F10 cells[24,25]. Neoantigens are tumor specific antigens created by somatic mutations [26]. We found that all AC-NP formulations, with the exception of mPEG AC-NPs, successfully captured neoantigens[24] (Figure 2c, Supplementary Table 1). Notably, AC-NPs also captured a number of damage associated molecular pattern proteins (DAMPs), a broad class of pro-inflammatory molecules that have been shown to potentiate immune response[27]. Notably, we found that our AC-NPs were capable of capturing histone proteins and alarmins (including HMGB1), both of which have been shown to enhance anti-tumor immune responses (Supplementary Table 1)[27]. Our data confirm that AC-NPs capture a myriad of TDPAs that are released after radiotherapy.

To investigate whether AC-NPs can improve immunotherapy, we employed a syngeneic mouse model of melanoma. Mice bearing bilateral B16F10 melanoma flank tumors underwent αPD-1 treatment. One of the tumors was irradiated (primary) and then injected with either PBS or AC-NPs, while the other tumor was shielded from radiation (secondary) (Figure 1; Supplementary Figure 2a). We assessed the immunotherapeutic efficacy and induction of the abscopal effect of different treatment regimens by measuring the growth rate of secondary tumors over time. We found that PLGA and Mal AC-NPs were able to significantly improve immunotherapy and the abscopal effect, eliciting the most robust therapeutic response across all treatment groups (Figure 3a, b). The greater therapeutic efficacy also translated into improved survival (Figure 3c). Impressively, the RT +αPD-1+PLGA AC-NP treatment strategy yielded a complete response rate (CRR) of 20%. These animals successfully rejected tumor re-challenge (subcutaneous injection of 100,000 B16F10 cells) 3 months later, demonstrating that this treatment strategy is capable of inducing durable anti-tumor immunity (Supplementary Figure 3). Of note, combining PLGA

and Mal AC-NPs into the same treatment regimen did not further enhance immunotherapy, suggesting that TDPAs commonly captured by these formulations may be responsible for the observed therapeutic benefit (Supplementary Figure 4). Moreover, PLGA and Mal AC-NP facilitated immunotherapeutic enhancement is lost following $CD8^+$ T cell depletion (Supplementary Figure 5). Importantly, we also found that AC-NPs improve immunotherapy in an orthotopic breast cancer tumor model (Supplementary Figure 6). Taken together, these data indicate that AC-NPs can indeed improve immunotherapy and promote the abscopal effect.

We next sought to determine the mechanism by which AC-NPs enhance the efficacy of cancer immunotherapy. As illustrated in Figure 1, successful immunotherapeutic tumor response requires the uptake and presentation of cancer antigens by APCs and the elicitation of an anti-cancer immune response. To confirm that AC-NPs are capable of delivering TDPAs to APCs, we injected rhodamine-labeled AC-NPs intratumorally and studied lymphatic drainage and distribution among lymph node residing dendritic cells, macrophages, and B-cells following radiotherapy. We found that AC-NPs injected into irradiated tumors readily trafficked to nearby tumor-draining lymph nodes (TDLNs) 16 hours post administration (Figure 4a, b). Importantly, PLGA and Mal AC-NPs accumulate at higher rates in professional antigen presenting dendritic cells ($CD11c^+$), macrophages ($F4/80^+$) and B-cells ($B220^+$) when compared to mPEG AC-NPs. Note that radiotherapy greatly enhances AC-NP uptake by APCs in resident lymph nodes (Supplementary Figure 7). This observation, taken together with the low accumulation of mPEG AC-NPs in APCs following radiotherapy, suggests that cellular uptake of AC-NPs requires capture of TDPAs released by radiotherapy.

To further characterize the method in which AC-NPs accumulate in lymph node residing APCs, we sought to assess whether AC-NPs were being actively transported by APCs from irradiated tumors to TDLNs or whether AC-NPs drain freely to lymph nodes prior to being taken up by APCs[28]. Our data demonstrate that the degree to which different AC-NP formulations utilize active versus passive transport varies based not only on AC-NP formulation, but also APC type (Supplementary Figure 8). For example, Mal AC-NPs are robustly taken up by dendritic cells in the irradiated tumor at 1 hour after irradiation and then demonstrate a concurrent decreased accumulation in dendritic cells within irradiated tumors and increased accumulation in dendritic cells within the TDLNs at 16 hours post-radiotherapy, suggesting successful dendritic cell mediated transport for this AC-NP formulation.

APCs play a pivotal role in initiating a successful adaptive immune response by processing foreign antigens and presenting peptide fragments to naïve T cells. Following antigen presentation, naïve $CD4^+$ and $CD8^+$ T cells become activated, experience clonal expansion, and gain helper functions (e.g. cytokine secretion) or cytotoxic capabilities. To determine whether the accumulation of AC-NPs carrying TDPAs would translate to successful T cell activation and expansion, the relative abundance of tumor infiltrating T cells was assessed in untreated secondary tumors of animals 16 days following radiotherapy. We found that animals treated with PLGA and Mal AC-NPs have more infiltrating $CD8^+$ T cells when compared to mice that did not receive AC-NP treatment (Figure 4c; Supplementary Figure

9). Additionally, the relative abundance of $CD4^+FOXP3^+$ regulatory T cells (T_{reg}), an immune suppressive T cell population that dampens antitumor immune responses, was substantially decreased in mice that received AC-NP treatment when compared to mice that did not receive AC-NPs. (Figure 4c; Supplementary Figure 9). Overall, the addition of AC-NPs to immunotherapy significantly increased intratumoral $CD8^+$ T/T_{reg} and $CD4^+$ T/T_{reg} ratios (Figure 4c), implying increased anti-tumor immunotherapeutic activity within the secondary tumor microenvironments of these animals. Although not significant, a similar trend was observed in the irradiated primary tumors of animals undergoing different treatment regimens. (Supplementary Figure 10). To further address whether AC-NPs are capable of eliciting systemic T cell activation, we assessed the *ex vivo* production of antitumor cytokine interferon-γ (IFN-γ)[29] by splenocytes harvested from mice that received different treatment regimens. We found that splenocytes isolated from animals in the PLGA and Mal AC-NP treatment arms demonstrated the highest percentage of IFN-γ secreting $CD4^+$ and $CD8^+$ T cells when stimulated with TDPAs (Figure 4d; Supplementary Figure 11). Importantly, negligible IFN-γ production was observed when T cell populations isolated from PLGA and Mal AC-NP treatment arms were stimulated with splenocyte lysates, indicating that the addition of these AC-NP formulations to standard immunotherapy promotes the production of a cancer specific immune response (Figure 4d; Supplementary Figure 12). To determine if AC-NP improve immunotherapy in an antigen-specific manner, we stimulated T cells isolated from animals undergoing different treatment regimens with neoantigen peptide fragments[24] identified in our mass spectrometry analysis (Actn4, Tubb3, Dag1, and Eef2). We found using flow cytometric analysis that T cells from PLGA and Mal AC-NP treatment arms demonstrate more robust IFN-γ production following neoantigen stimulation. (Supplementary Figure 12). To further assess neoantigen stimulation, we also performed an Enzyme-Linked ImmunoSpot (ELISPOT) assay using splenocytes isolated from all treatment arms. We found that PLGA and Mal AC-NP treatment arms trended towards having the most robust T cell activation following exposure to Actn4 and Tubb3 (Supplementary Figure 13). Collectively, our results demonstrate that AC-NPs used in combination with radiotherapy and immunotherapy increased anti-cancer $CD8^+$ and $CD4^+$ effector neoantigen-specific T cell quantity and quality.

Finally, to confirm that the improved immunotherapeutic response and abscopal effect are attributable to AC-NP administration, we examined the effect of direct administration of AC-NPs coated with TDPA *ex vivo* to tumor bearing mice receiving αPD-1 immunotherapy treatment (Supplementary Figure 2b). Despite lower accumulation in lymph node residing APCs (Supplementary Figure 14), we found that administration of both Mal AC-NPs and PLGA AC-NPs coated with TDPAs *ex vivo* significantly delayed tumor growth (Figure 5a, b) and increased survival time (Figure 5c). As with the therapeutic enhancement observed in our *in vivo* abscopal studies, PLGA and Mal AC-NP facilitated immunotherapeutic enhancement of cancer vaccination is lost following $CD8^+$ T cell depletion (Supplementary Figure 15).

In summary, we have developed biodegradable and biocompatible AC-NPs that can improve cancer immunotherapy and induce the abscopal effect. We show that AC-NPs enhance the presentation of TDPAs by APCs, resulting in a more robust activation of $CD8^+$ T cells. A continuing challenge that limits the effectiveness of cancer therapy is tumor heterogeneity

within individual patients and among patient populations. Traditional strategies of enhancing the immunotherapeutic response by administering one or several "chosen" antigens remain unsuccessful[30], perhaps because this approach fails to account for tumor cell diversity. In contrast to traditional methods, our novel strategy exposes the immune system to a wide variety of TDPAs in a patient specific manner. This treatment approach carries important implications for the advancement of personalized medicine. Importantly, our AC-NP based approach is synergistic with existing clinical immunotherapy treatment regimens, and our AC-NPs formulations contain FDA generally regarded as safe (GRAS) materials, allowing for rapid clinical translation. Our work can potentially facilitate precision medicine with personalized immunotherapy and improve the outcomes of patients suffering from extensive metastatic disease.

Methods

Cell Lines

The B16-F10 and 4T1 cell lines were acquired from ATCC, where these lines were authenticated using morphology, karyotyping, and PCR based approaches and tested for mycoplasma. B16-F10 cells were cultured in Dulbecco's Modified Eagle's Medium (DMEM) (Gibco) supplemented with 10% fetal bovine serum (Mediatech), 100 U ml^{-1} penicillin and 100 μg ml^{-1} streptomycin (Mediatech), and 2mML-glutamine (Gibco). The cell cultures were maintained below 50% confluence and early-passage cultures (between 4 and 9) were utilized for experiments.

Materials

PLGA (AP059; LA:GA=50:50 (w:w); M_W: 45,000–55,000 Da), mPEG-PLGA (AK037; LA:GA=50:50 (w:w); M_W: ~25,000 Da), PLGA-PEG-NH_2 (AI058; M_W: ~17,000 Da), PLGA-PEG-Mal (AI052; LA:GA=75:25; M_W: ~63,400 Da), and Poly(lactide-co-glycolide)-Rhodamine B (PLGA-Rb) (AV011; LA:GA=50:50; M_n=10,000–30,000 Da) were obtained from Polyscitech®. All other chemicals were obtained from Sigma-Aldrich unless otherwise noted.

Collagenase/Hyaluronidase and Bovine Pancreas DNase I-PBS solution were obtained from Stemcell Technologies. LIVE/DEAD® Fixable Yellow Dead Cell Stain Kit and ACK lysis buffer were obtained from Life Technology. Recombinant Murine IL-2 was obtained from PeproTech. αPD-1 (clone: RMP1-14) was from BioXcell. The peptides Actn4 (NHSGLVTFQAFIDVMSRETTDTDTADQ), Eef2 (FVVKAYLPVNESFAFTADLRSNTGGQA), Tubb3 (FRRKAFLHWYTGEAMDEMEFTEAESNM), or Dag1 (TAVITPPTTTTKKARVSTPKPATPSTD) were obtained from peptide 2.0 (Chantilly, VA). All antibodies used for flow cytometric assays are listed in the Supplementary Table 2.

Preparation of Antigen Capturing Nanoparticles (AC-NPs)

The NPs were synthesized using a previously reported nanoprecipitation technique[31]. Briefly, to prepare the PLGA NPs, PLGA (4 mg/mL) in acetonitrile (ACN) was added dropwise into 3 mL of endotoxin free water and stirred at room temperature under a vacuum

until the ACN completely evaporated (approximately 3 hours). To prepare the DOTAP core-shell NPs[32], PLGA (4 mg/mL) in ACN was added dropwise into 3 mL of 4% ethanol solution containing lecithin/DOTAP (7:3 molar ratio) with a weight ratio of 15% to the PLGA polymer solution pre-heated to 55.0 °C. This solution was vortexed for 3 min and stirred at room temperature under a vacuum until the ACN completely evaporated. To prepare the X AC-NPs (X= mPEG, NH_2 or Mal (Maleimide)), PLGA-PEG-X (20 mg/mL) in ACN was added dropwise into 3 mL of endotoxin free water and stirred at room temperature under vacuum until the ACN completely evaporated. The resulted NPs were used either for intratumoral injection in abscopal experiment or for preparing TDPAs coated AC-NPs *ex vivo* in the next step.

In Vitro Formulation of Antigen Capturing Nanoparticles (AC-NPs) coated with TDPAs

Preparing Tumor Antigens from Irradiated B16-F10 Cells—B16-F10 cells were seeded in T175 flask containing 25 mL of culture media and incubated overnight at 37°C. Cells were then washed with PBS or plain medium and irradiated with 100 Gy photon radiation delivered using a Precision X-RAD 320 (Precision X-ray, Inc.) machine operating at 320 kvp and 12.5 mA. Subsequently, the B16-F10 cells were incubated in media without FBS for 48 hours. Following incubation, the supernatant was collected and spun down at 200 g for 5 min to remove insoluble cellular debris.

Preparation of AC-NP coated with TDPAs *Ex Vivo*—AC-NPs were incubated with antigen containing supernatants prepared from irradiated B16-F10 cells as described above. Specifically, 20 mg of each AC-NP formulation was mixed with the 20 mL of tumor antigens from 10 million irradiated B16-F10 cells. Following incubation, AC-NPs were washed with endotoxin free H_2O or PBS using ultra-filtration (500–800g, Amicon Ultra, Ultracel membrane with 100, 000 NMWL, Millipore, Billerica, MA). Pre-loaded AC-NPs prepared using this method were either characterized or used for cancer immunotherapy assays *in vivo*.

Vials and stir bars for NPs preparation were autoclaved and washed with acetone and ACN before use. All NPs were made under endotoxin-free condition.

Characterization of AC-NPs Before and After *Ex Vivo* Antigen Capture—Changes in AC-NP size after antigen capture was determined using intensity-average diameter (D_h, also known as hydrodynamic diameter) of NPs. Changes in the mean zeta potential (mean ζ) of AC-NPs following antigen capture was analyzed by dynamic light scattering and aqueous electrophoresis using a Zetasizer Nano ZS Instrument (Malvern, Inc.). Prior to the measurements, NPs were diluted to 0.5 mg/mL with DI H_2O. The amount of protein bound by AC-NPs was determined using BCA analysis. Specifically AC-NPs were incubated in a supernatant containing TDPAs and subsequently removed. The total protein uptake by AC-NPs was determined by subtracting the protein concentration in the supernatant after AC-NP capture from the protein concentration in the supernatant before capture. All measurements were based on the average of three separate measurements (Supplementary Fig. 1).

Identification of Proteins Captured by each AC-NP formulation by LC/MS/MS Analysis—Following preparation, pre-loaded AC-NPs were first washed with Centrifugal Device (300,000 NMWL, Nanosep) and the solutions were then diluted 5-fold with ACN. ACN was then evaporated under vacuum and the remaining solution was centrifuged at 200 g for 5 min. The supernatant was collected and processed for mass spectrum analysis using a previously established FASP (Filter assisted sample preparation) protocol[33], a process that includes reduction, alkylation, and digested with trypsin. The peptides were then extracted, lyophilized, and resuspended in 2% acetonitrile/98% (0.1% formic acid). This peptide containing solution was then loaded onto a 2 cm long × 360 μm o.d. × 100 μm i.d. microcapillary fused silica pre-column packed with Magic 5 μm C18AQ resin (Michrom Biosciences). After sample loading, the pre-column was washed with 95% Solvent A (0.1% aqueous formic acid)/5% Solvent B (0.1% formic acid in ACN) for 20 min at a flow rate of 2 uL/min. The pre-column was then connected to a 360 μm o.d. × 75 μm i.d. analytical column packed with 22 cm of 5 μm C18 resin. The peptides were eluted at a flow rate of 250 nL/min by increasing the percentage of solvent B to 40% with a Nano-Acquity HPLC solvent delivery system (Waters Corp.). The LC system was directly connected through an electrospray ionization source interfaced to an LTQ Orbitrap Velos ion trap mass spectrometer (Thermo Fisher Scientific). The mass spectrometer was controlled by Xcalibur software and operated in the data-dependent mode in which the initial MS scan recorded the mass to charge (m/z) ratios of ions over the range 400–2000. The 10 most abundant ions were automatically selected for subsequent collision-activated dissociation. Each sample was analyzed by LC-MS/MS and the 2 runs were denoted R1 and R2.

Raw data files were processed using Proteome Discoverer (PD) version 1.4 (Thermo Scientific). Peak lists were searched against a Reviewed Mouse Uniprot database (downloaded in 2016) using Sequest. The following parameters were used to identify tryptic peptides for protein identification: 10 ppm precursor ion mass tolerance; 0.6 Da product ion mass tolerance; up to two missed trypsin cleavage sites; carbamidomethylation of Cys was set as a fixed modification; oxidation of Met was set as a variable modification. Peptide spectral matches (PSMs) for both runs for each sample were averaged. The relative abundance of proteins captured by each AC-NP formulation was determined by dividing the PSM values from each sample by the average PSMs across all samples for each protein (mean normalization).

The Percolator node within PD was used to calculate peptide false discovery rates (FDR), and a 5% FDR was used to filter all results. Only proteins identified in both runs with ≥2 peptides were reported. The mass spectrometry proteomics data have been deposited to the ProteomeXchange Consortium via the PRIDE[34] partner repository with the dataset identifier PXD006049. The proteins captured by different AC-NPs formulations were compared and the overall *P* value was calculated by one-way analysis of variance (ANOVA) with Tukey post-test using the GraphPad Prism 5.0. *P* value: *, $P<0.05$; **, $P<0.01$; ***, $P<0.005$.

Identification of neoantigens[35] Captured by each AC-NP formulation—Neoantigen-containing proteins in the B16F10 mouse model were predicted *in silico* using our previously described pipeline[24, 25]. Note that only combinations of adjacent missense mutations supported on the same read of WES data were considered and only neoantigens

predicted in four of four biological replicates were included in our analysis. This neoantigen list was combined with a previously published list of neoantigens[24, 36]. Briefly, a list of nanoparticle bound proteins obtained from the mass spec data was run through a python script to find proteins with at least one predicted neoantigen or previously identified neoantigen.

In Vivo Efficacy Studies in Mice

For all *in vivo* assays, six- to eight-week-old female C57BL/6 mice (The Jackson Laboratory) with the body weight of 20 grams were used. Sample sizes were calculated based on our preliminary data. We calculated an effect size of 1.821. The nonparametric analog of this effect size can be stated in terms of p_1=Pr (X<Y), or an observation in Group X is less than an observation in Group Y when H_1 is true. The null hypothesis being tested is p_1=0.5. For effect size 1.821, p_1=0.099. A sample size of at least 8 in each group will have 80% power to detect a probability of 0.099 that an observation in Group X is less than an observation in Group Y, using a Wilcoxon (Mann-Whitney) rank-sum test, with a 0.05 two-sided significance level. Mice were assigned to treatment groups based on cage numbers. The groups were not blinded. The efficacy data is representative one from three independent experiments. All animal work was approved and monitored by the University of North Carolina Animal Care and Use Committee.

Efficacy of AC-NPs in Improving the Abscopal Effect—For abscopal studies, 50,000 B16-F10 cells were suspended in DMEM, mixed with an equal volume of Matrigel (BD Biosciences), and subcutaneously injected on the left flank of C57BL/6 mice on day 0 (primary tumors) and the right flank on day 3 (secondary tumors). The left flank tumors (primary tumors) were irradiated with 8 Gy[37, 38] on days 8, 9, and 10 using a X-RAD 320. A lead shield protected the rest of the animal. αPD-1 blocking antibody (10 mg/kg) was intraperitoneally injected into animals on days 5, 8, and 11. AC-NPs (2 mg in 100 μL PBS) were injected into primary tumors on days 10, 11, and 12. Note PLGA AC-NPs were suspended in DI H_2O containing 0.05% polyvinyl alcohol (PVA). The detailed schedule can be found in Supplementary Fig. 2a. CD 8 depletion assays were conducted by administering anti-CD8 (clone: 2.43) antibody two days prior to tumor inoculation, on the day of tumor inoculation, and every four days following tumor inoculation for the duration of experiment. Animals were sacrificed when an aspect of tumor lengths reached a size of 1.5 cm. The same methodology used for the B16-F10 xenograft model was also used for the 4T1 orthotopic model with the exception that in these studies tumors were created by injecting 50,000 4T1 cells into the mammary pads of mice.

TDPAs coated AC-NPs as Cancer Vaccines—For vaccine studies, 50,000 B16-F10 cells in DMEM were mixed with an equal volume of Matrigel (BD Biosciences) and subcutaneously injected on the left flank of C57BL/6 mice on day 0. Pre-loaded AC-NPs (2 mgs) or free tumor antigens were subcutaneously injected into the right flank of mice on days 3, 6, and 9. Free tumor antigen injections were prepared by concentrating the supernatant from 1 million irradiated B16-F10 cells (the same amount and composition of supernatant used for AC-NP loading). The supernatant was concentrated using ultra-filtration through an Ultracel membrane (100,000 NMWL Millipore). αPD-1 (clone:

RMP1-14) blocking antibody (5 mg/kg) was intraperitoneally injected into animals on days 3, 6 and 9. The detailed schedule can be found in Supplementary Fig. 2b. As before, CD 8 depletion assays were conducted by administering anti-CD8 (clone: 2.43) antibody two days prior to tumor inoculation, on the day of tumor inoculation, and every four days following tumor inoculation for the duration of experiment. Animals were sacrificed when an aspect of tumors exceeded 2.0 cm in length.

Tumor Volume Measurements

Two perpendicular diameters were measured with a caliper and tumor volumes were calculated using the formula $V = 0.52 \times a \times b^2$, where a and b are the larger and smaller diameters, respectively. The tumor volumes were assessed every 2–3 days. Two independent researchers assessed tumor volume over time with one researcher blinded to the treatment group assignments. Statistical differences in average tumor growth curves were determined by two-way ANOVA using variables of time and volume. Differences in survival in each group were determined using the Kaplan-Meier method and the overall P value was calculated by the log-rank test using the GraphPad Prism 5.0. P value: *, $P<0.05$; **, $P<0.01$; ***, $P<0.005$.

Uptake of AC-NPs by Antigen Presenting Cells in Irradiated Tumor and Lymph Nodes

For tumor inoculation, 50,000 B16-F10 cells in DMEM were mixed with an equal volume of Matrigel (BD Biosciences) and subcutaneously injected on the left flank of C57BL/6 mice on day 0. The tumor was irradiated with 8 Gy using a Precision X-RAD 320 (Precision X-ray, Inc.) on days 8, 9 and 10. The rest of the body was protected with lead shielding. After the last dose of radiation on day 10, rhodamine B-labeled AC-NPs (2mg) were injected into the irradiated tumor. The rhodamine B-labeled AC-NPs were prepared as described above with the exception that 5% wt/wt of PLGA-Rb was used for nanoprecipitation. The concentration of all labeled AC-NPs was quantified with a fluorescence spectrum photometer. The irradiated tumor and the nearby TDLNs were dissected 1 hour or 16 hours post treatment for flow cytometric analysis. Rhodamine B-labeled AC-NPs within lymph nodes were imaged with an IVIS imaging system. Uptake of AC-NPs into antigen presenting cells was assessed by flow cytometric analysis of single cell suspensions. These were stained with anti-mouse CD11c, F4/80, and B220 (Supplementary Table 1). The drainage of AC-NPs in vaccination studies to APCs in nearby lymph nodes was assessed by subcutaneously injecting TDPAs coated rhodamine B-labeled AC-NPs and collecting nearby lymph nodes 1 hour or 16 hours post injection for flow cytometric analysis. P value was calculated by Mann Whitney test using the GraphPad Prism 5.0. P value: *, $P<0.05$; **, $P<0.01$; ***, $P<0.005$.

Flow Cytometric Analysis of Relative Abundance of Tumor Infiltrating T Cell Populations

B16-F10 tumors were harvested on day 16–18 post tumor inoculation for flow cytometric analysis of *in vivo* experiments. Single cell suspensions were prepared using collagenase/hyaluronidase and DNase and red blood cells were lysed using ACK Lysis Buffer (Life Technologies). Live/Dead fixable yellow dead cell staining kit (Life Technologies) was applied for live/dead cell discrimination. Before surface staining, samples were incubated with Fc Block for 5 min on ice, followed by surface staining with anti-mouse CD45, CD3, CD8, CD4 (Supplementary Table 1). Cells were then fixed, permeabilized, and stained for

intracellular FOXP3 (eBioscience). T effector cells were phenotyped as $CD8^+$ and regulatory T cells (T_{reg} cells) as $CD4^+FOXP3^+$. All flow cytometric analysis was done using a Beckman Coulter CyAn ADP and analyzed using software Summit 5.2. Flow cytometric data analysis was performed in a blinded fashion. Two independent researchers performed collection and analysis of flow cytometric data. Differences were compared and the overall *P* value was calculated by Mann Whitney test using the GraphPad Prism 5.0. (*P* value: *, $P<0.05$; **, $P<0.01$; ***, $P<0.005$.) The representative plots of relative abundance of tumor infiltrating T cells were showed in Supplementary Fig. 9.

Flow Cytometric Analysis Evaluating IFN-γ Production by T Cells following Stimulation *Ex Vivo*

Splenocytes were harvested on day 16–18 post B16-F10 tumor inoculation and plated for culture. The splenocytes were re-stimulated with TDPAs isolated from B16F10 lysates or neoantigens (Actn4, Eef1, Tubb3, Dag1) for 72 hours. After stimulation, splenocytes were washed and stained. Single cell suspensions were blocked with Fc Block for 5 minutes on ice and then stained with anti-mouse CD3, CD8, CD4 (Supplementary Table 1). Live/dead fixable yellow dead cell stain kit (Life Technologies) was applied for live/dead cell discrimination. For surface staining, samples were first incubated with Fc block for 5 min on ice and stained with anti-mouse CD3, CD8, CD4 (Supplementary Table 1). Cells were then fixed, permeabilized, and stained for intracellular IFN-γ. All flow cytometric analysis was done using a Beckman Coulter CyAn ADP and analyzed using software Summit 5.2. The data were presented as the percentage of $CD8^+IFN\text{-}\gamma^+$ in $CD8^+$ cells, and the percentage of $CD4^+IFN\text{-}\gamma^+$cells in $CD4^+$ cells. Differences were compared and the overall *P* value was calculated by Mann Whitney test using the GraphPad Prism 5.0. (*P* value: *, $P<0.05$; **, $P<0.01$; ***, $P<0.005$.) The representative plots of relative abundance IFN-γ production T cells were showed in Supplementary Fig. 10.

Assessment Antigen Specific Immunity using ELISPOT

For analysis of interferon gammar (IFN-γ) production, spleens were harvested on day 16–18 post B16-F10 tumor inoculation from animals in all treatment groups. Single cell suspensions were prepared. IFN-γ production was measured with BD™ ELISPOT assay system (BD Pharmingen, San Diego, CA) according to the manufacturer's instructions. Briefly, the splenocytes were seeded at different cell densities into 96-well plates that were pretreated with capture antibody and incubated in RPMI 1640 media supplemented with NEAA and 10 μM predicted peptides (Actn4, Eef1, Tubb3, or Dag1) at 37°C. After 18 hours, cells were removed and production of IFN-γ was detected by adding detection antibody followed by enzyme conjugation. Signals were developed using BD™ ELISPOT substrate set and plates were evaluated in high resolution using automated ELISPOT reader systems from Zeiss (ELISPOT) and AID (Fluorospot).

Data availability

All relevant data within the text and supplementary information are available from the corresponding authors upon request.

Supplementary Material

Refer to Web version on PubMed Central for supplementary material.

Acknowledgments

The authors would like to acknowledge Dr. David Smalley at the Michael Hooker Proteomics Center for her assistance with mass spectrum data analysis (CA016086). The authors also acknowledge the UNC Flow Cytometry Core Facility (P30 CA016086). The authors would also like to thank our funding sources. A.Z.W., J.E.T., S.T., and J.M.D are supported by funding from the National Institutes of Health/National Cancer Institute (U54CA198999, Carolina Center of Cancer Nanotechnology Excellence (CCNE)-Nano Approaches to Modulate Host Cell Response for Cancer Therapy). B.V. is supported by funding from UNC University Cancer Research Fund, Paul Calabresi Oncology K12 Award and UNC CCNE Pilot Grant. A.Z.W. is also supported by funding from the NIH/NCI (U54 CA151652 and R01 CA178748) for this work. A.Z.W. was also supported by funding from the NIH/NCI (R21 CA182322). This work was also supported by a generous gift from Mr. And Mrs. Edward Barclay.

References

1. Couzin-Frankel J. Breakthrough of the year 2013. Cancer immunotherapy. Science. 2013; 342:1432–3. [PubMed: 24357284]
2. Postow MA, et al. Immunologic correlates of the abscopal effect in a patient with melanoma. N Engl J Med. 2012; 366:925–31. [PubMed: 22397654]
3. Twyman-Saint Victor C, et al. Radiation and dual checkpoint blockade activate non-redundant immune mechanisms in cancer. Nature. 2015; 520:373–7. [PubMed: 25754329]
4. McNutt M. Cancer immunotherapy. Science. 2013; 342:1417. [PubMed: 24357273]
5. Pardoll DM. The blockade of immune checkpoints in cancer immunotherapy. Nat Rev Cancer. 2012; 12:252–64. [PubMed: 22437870]
6. Brahmer JR, et al. Safety and activity of anti-PD-L1 antibody in patients with advanced cancer. N Engl J Med. 2012; 366:2455–65. [PubMed: 22658128]
7. Hamid O, et al. Safety and tumor responses with lambrolizumab (anti-PD-1) in melanoma. N Engl J Med. 2013; 369:134–44. [PubMed: 23724846]
8. Hodi FS, et al. Improved survival with ipilimumab in patients with metastatic melanoma. N Engl J Med. 2010; 363:711–23. [PubMed: 20525992]
9. Topalian SL, et al. Safety, activity, and immune correlates of anti-PD-1 antibody in cancer. N Engl J Med. 2012; 366:2443–54. [PubMed: 22658127]
10. Wolchok JD, et al. Nivolumab plus ipilimumab in advanced melanoma. N Engl J Med. 2013; 369:122–33. [PubMed: 23724867]
11. Garon EB, et al. Pembrolizumab for the treatment of non-small-cell lung cancer. N Engl J Med. 2015; 372:2018–28. [PubMed: 25891174]
12. Formenti SC, Demaria S. Combining radiotherapy and cancer immunotherapy: a paradigm shift. J Natl Cancer Inst. 2013; 105:256–65. [PubMed: 23291374]
13. Sharabi AB, Lim M, DeWeese TL, Drake CG. Radiation and checkpoint blockade immunotherapy: radiosensitisation and potential mechanisms of synergy. Lancet Oncology. 2015; 16:E498–E509. [PubMed: 26433823]
14. Chan JK, et al. Alarmins: awaiting a clinical response. J Clin Invest. 2012; 122:2711–9. [PubMed: 22850880]
15. Curtin JF, et al. HMGB1 mediates endogenous TLR2 activation and brain tumor regression. PLoS Med. 2009; 6:e10. [PubMed: 19143470]
16. Apetoh L, et al. Toll-like receptor 4-dependent contribution of the immune system to anticancer chemotherapy and radiotherapy. Nat Med. 2007; 13:1050–9. [PubMed: 17704786]
17. Fang RH, Kroll AV, Zhang L. Nanoparticle-Based Manipulation of Antigen-Presenting Cells for Cancer Immunotherapy. Small. 2015; 11:5483–96. [PubMed: 26331993]
18. Smith DM, Simon JK, Baker JR Jr. Applications of nanotechnology for immunology. Nat Rev Immunol. 2013; 13:592–605. [PubMed: 23883969]

19. Goldberg MS. Immunoengineering: How Nanotechnology Can Enhance Cancer Immunotherapy. Cell. 2015; 161:201–204. [PubMed: 25860604]
20. Irvine DJ, Hanson MC, Rakhra K, Tokatlian T. Synthetic Nanoparticles for Vaccines and Immunotherapy. Chem Rev. 2015; 115:11109–46. [PubMed: 26154342]
21. Shao K, et al. Nanoparticle-based immunotherapy for cancer. ACS Nano. 2015; 9:16–30. [PubMed: 25469470]
22. Kim J, et al. Injectable, spontaneously assembling, inorganic scaffolds modulate immune cells in vivo and increase vaccine efficacy. Nat Biotechnol. 2015; 33:64–72. [PubMed: 25485616]
23. Jokerst JV, Lobovkina T, Zare RN, Gambhir SS. Nanoparticle PEGylation for imaging and therapy. Nanomedicine (Lond). 2011; 6:715–28. [PubMed: 21718180]
24. Kreiter S, et al. Mutant MHC class II epitopes drive therapeutic immune responses to cancer. Nature. 2015; 520:692–6. [PubMed: 25901682]
25. Kardos J, et al. Claudin-low bladder tumors are immune infiltrated and actively immune suppressed. JCI Insight. 2016; 1:e85902. [PubMed: 27699256]
26. Schumacher TN, Schreiber RD. Neoantigens in cancer immunotherapy. Science. 2015; 348:69–74. [PubMed: 25838375]
27. Krysko DV, et al. Immunogenic cell death and DAMPs in cancer therapy. Nat Rev Cancer. 2012; 12:860–75. [PubMed: 23151605]
28. Bachmann MF, Jennings GT. Vaccine delivery: a matter of size, geometry, kinetics and molecular patterns. Nat Rev Immunol. 2010; 10:787–96. [PubMed: 20948547]
29. Wang C, Sun W, Wright G, Wang AZ, Gu Z. Inflammation-Triggered Cancer Immunotherapy by Programmed Delivery of CpG and Anti-PD1 Antibody. Adv Mater. 2016; 28:8912–8920. [PubMed: 27558441]
30. Melief CJ, van Hall T, Arens R, Ossendorp F, van der Burg SH. Therapeutic cancer vaccines. J Clin Invest. 2015; 125:3401–12. [PubMed: 26214521]
31. Govender T, Stolnik S, Garnett MC, Illum L, Davis SS. PLGA nanoparticles prepared by nanoprecipitation: drug loading and release studies of a water soluble drug. J Control Release. 1999; 57:171–85. [PubMed: 9971898]
32. Zhang L, et al. Self-assembled lipid--polymer hybrid nanoparticles: a robust drug delivery platform. ACS Nano. 2008; 2:1696–702. [PubMed: 19206374]
33. Wisniewski JR, Zougman A, Nagaraj N, Mann M. Universal sample preparation method for proteome analysis. Nat Methods. 2009; 6:359–62. [PubMed: 19377485]
34. Vizcaino JA, et al. 2016 update of the PRIDE database and its related tools. Nucleic Acids Res. 2016; 44:11033. [PubMed: 27683222]
35. Gubin MM, Artyomov MN, Mardis ER, Schreiber RD. Tumor neoantigens: building a framework for personalized cancer immunotherapy. J Clin Invest. 2015; 125:3413–21. [PubMed: 26258412]
36. Castle JC, et al. Exploiting the mutanome for tumor vaccination. Cancer Res. 2012; 72:1081–91. [PubMed: 22237626]
37. Dewan MZ, et al. Fractionated but not single-dose radiotherapy induces an immune-mediated abscopal effect when combined with anti-CTLA-4 antibody. Clin Cancer Res. 2009; 15:5379–88. [PubMed: 19706802]
38. Martinov T, Fife BT. Fractionated radiotherapy combined with PD-1 pathway blockade promotes CD8 T cell-mediated tumor clearance for the treatment of advanced malignancies. Ann Transl Med. 2016; 4:82. [PubMed: 27004229]

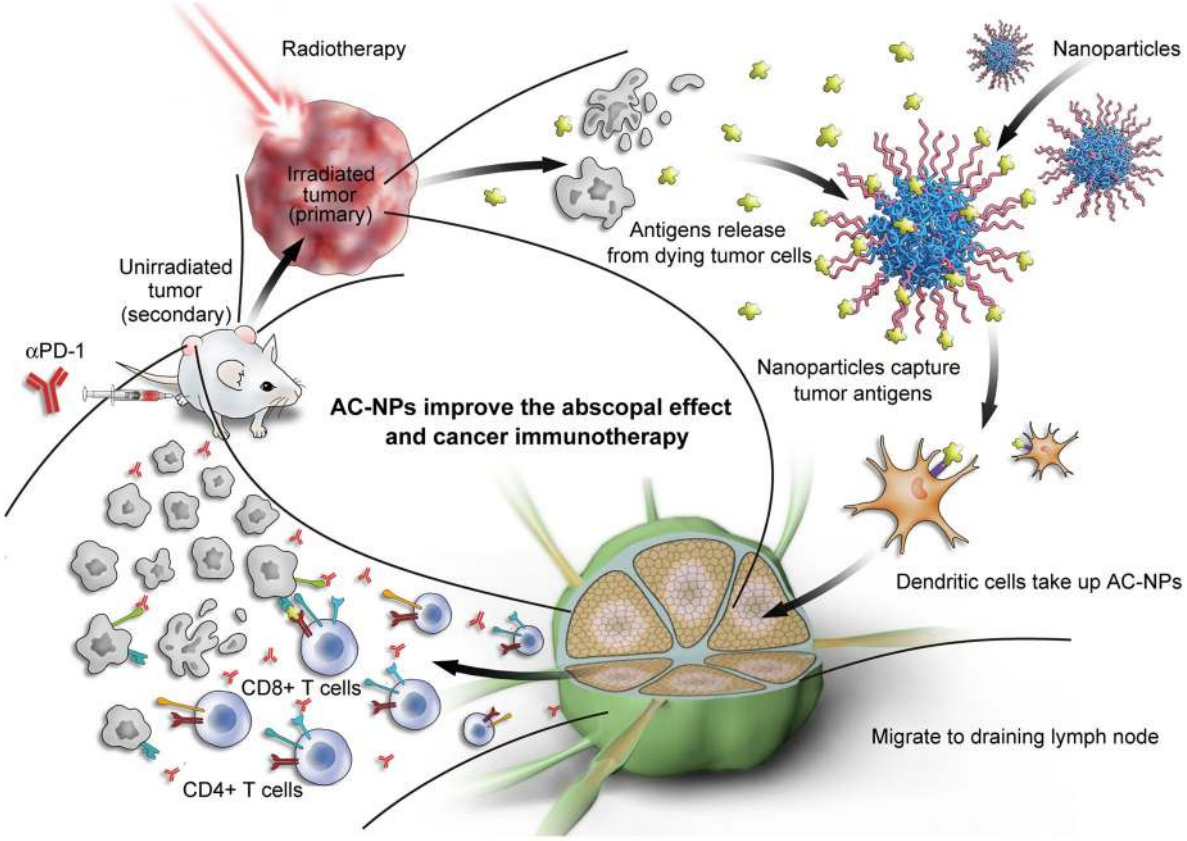

Figure 1.

Schematic depiction of utilizing antigen-capturing nanoparticles (AC-NPs) to improve cancer immunotherapy. Following radiotherapy, AC-NPs bind to tumor antigens and improve their presentation to dendritic cells. The improved antigen-presentation and immune activation is synergistic with αPD-1 treatment.

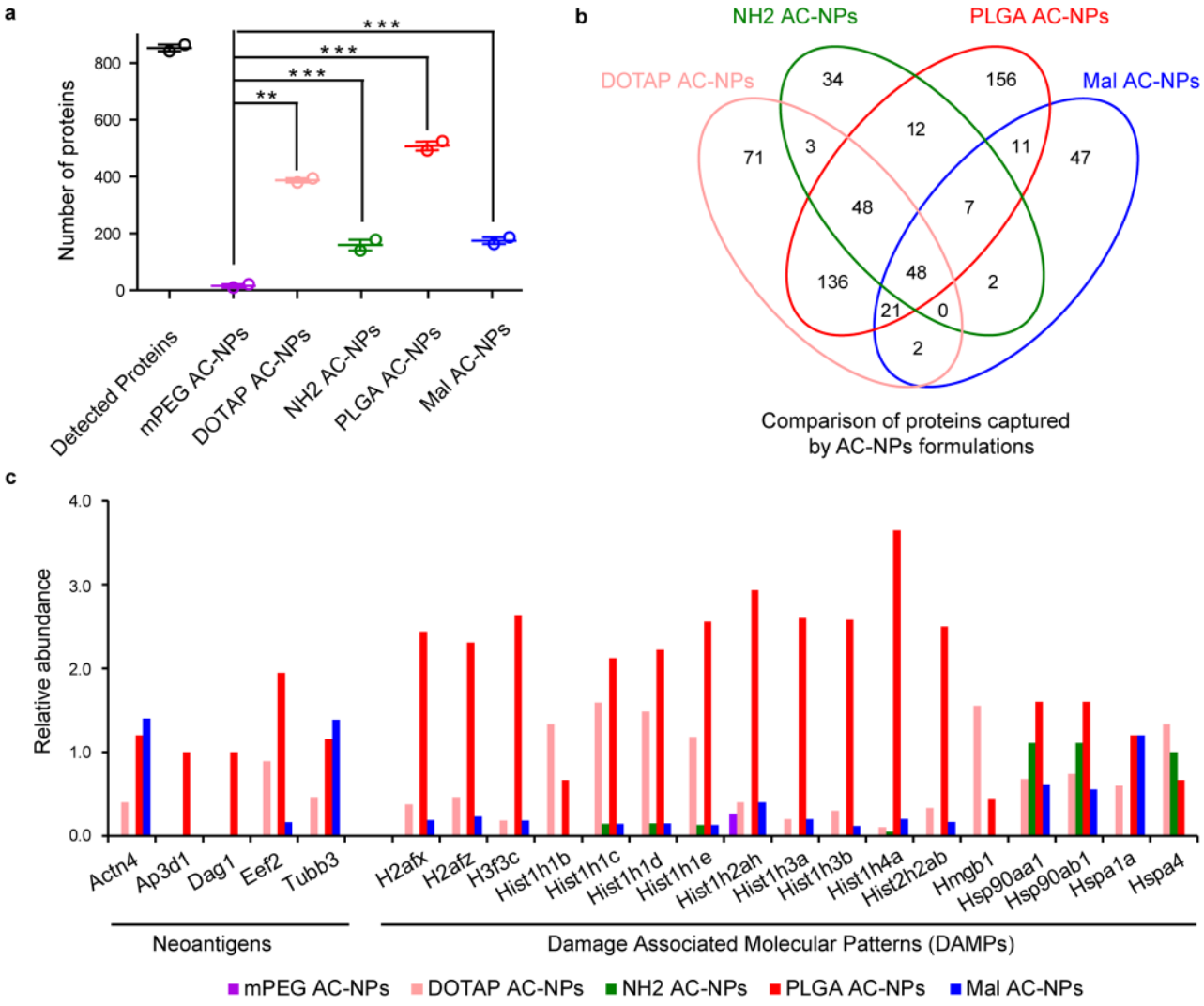

Figure 2.

The capture of cancer derived proteins by AC-NPs is dependent upon their surface chemistry. (a) Number of unique proteins bound to AC-NPs. (b) Comparison of proteins bound to AC-NPs with different surface chemistries. (c) The relative abundance of neoantigens and DAMPs captured by AC-NPs. The number of proteins captured by AC-NPs was compared by one-way analysis of variance (ANOVA) with Tukey's post-test. Data represent mean ±standard error of the mean (SEM). *P* value (*, $P<0.05$; **, $P<0.01$; ***, $P<0.005$)

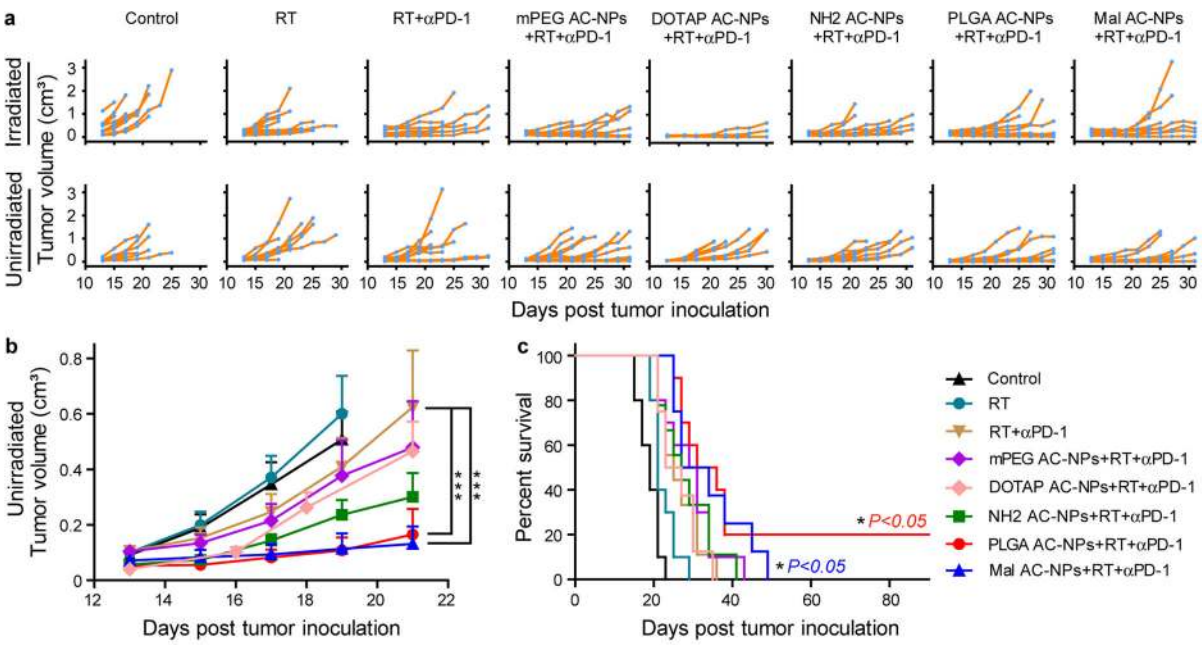

Figure 3.

AC-NPs can improve immunotherapy and the abscopal effect in B16-F10 xenografts. (a) Growth curves of irradiated (primary) and unirradiated (secondary) tumors in individual mice treated with immunotherapy and AC-NP formulations. (b) Average tumor growth curves of unirradiated (secondary) tumors in mice treated in (a). (c) Survival curves of the mice in (a). (Control, n=10; RT, n=10; RT+αPD-1, n=9; mPEG AC-NPs+RT+αPD-1, n=10; DOTAP AC-NPs+RT+αPD-1, n=8; NH2 AC-NPs+RT+αPD-1, n=9; PLGA AC-NPs+RT +αPD-1, n=10; Mal AC-NPs+RT+αPD-1, n=8). Tumor growth over time was compared by two-way analysis of variance (ANOVA) with Bonferroni correction. Data represent mean ± standard error of the mean (SEM). Differences in survival were determined for each group by the Kaplan-Meier method and the overall *P* value was calculated by the log-rank test. *P* value (*, $P<0.05$; **, $P<0.01$; ***, $P<0.005$)

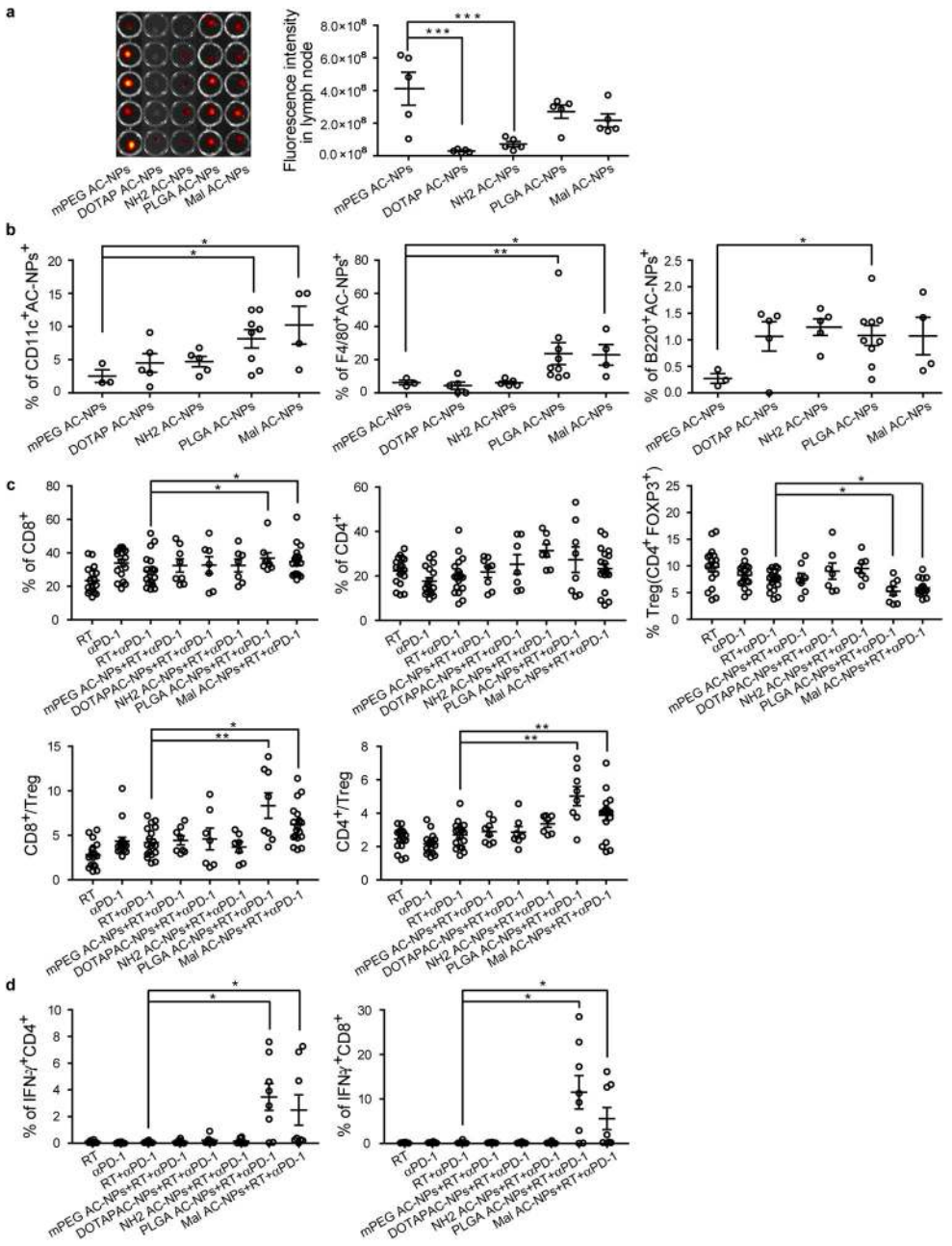

Figure 4.

AC-NPs facilitate antigen uptake by APCs and increase immune activation. (a) Image of TDLNs after intratumoral injection of fluorescently-labeled AC-NPs and quantification of fluorescence intensity in these lymph nodes following the primary tumor with radiotherapy. (n=5) (b) Flow cytometric analysis quantifying the percent of antigen presenting dendritic cells ($CD11c^+$), macrophages ($F4/80^+$), and B cells ($B220^+$) with fluorescently-labeled AC-NPs in TDLNs after raiotherapy (mPEG AC-NPs+RT, n=3; DOTAP AC-NPs+RT, n=5; NH2 AC-NPs+RT, n=5; PLGA AC-NPs+RT, n=9; Mal AC-NPs+RT, n=4). (c) Flow cytometric analysis assessing the relative abundance of $CD8^+$, $CD4^+$, and $CD4^+FOXP3^+$ T cell

subpopulations in secondary tumors (RT, n=17; αPD-1, n=17; RT+αPD-1, n=18; mPEG AC-NPs+RT+αPD-1, n=8; DOTAP AC-NPs+RT+αPD-1, n=7; NH2 AC-NPs+RT+αPD-1, n=7; PLGA AC-NPs+RT+αPD-1, n=8; Mal AC-NPs+RT+αPD-1, n=18). T cells were defined as being $CD45^+CD3^+$. (d) Flow cytometric analysis evaluating IFN-γ secreting T cells in spleens of animals treated with AC-NPs and subsequently stimulated *ex vivo* with cancer derived antigens (RT, n=6; αPD-1, n=6; RT+αPD-1, n=8; mPEG AC-NPs+RT +αPD-1, n=8; DOTAP AC-NPs+RT+αPD-1, n=8; NH2 AC-NPs+RT+αPD-1, n=8; PLGA AC-NPs+RT+αPD-1, n=8; Mal AC-NPs+RT+αPD-1, n=8). T cells in this assay were defined as $CD3^+$. Statistical significance was assessed using Mann Whitney test. Data represent mean ±standard error of the mean (SEM). *P* value (*, $P<0.05$; **, $P<0.01$; ***, $P<0.005$)

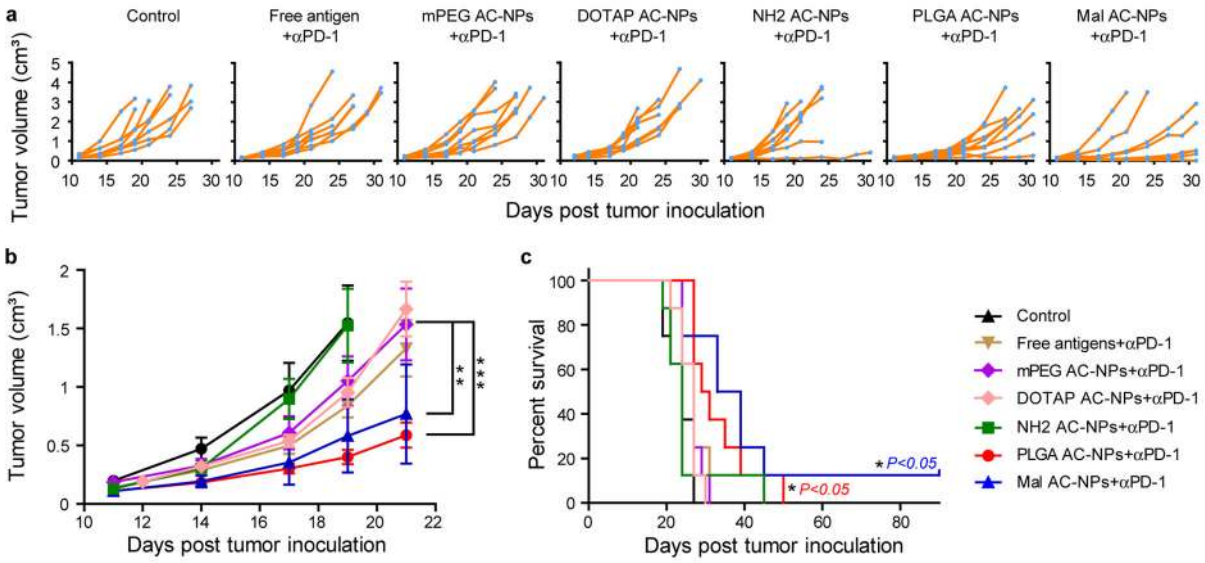

Figure 5.

TDPAs coated AC-NPs enhance the efficacy of cancer vaccination based immunotherapy. (a) Tumor growth curves of individual animals treated with immunotherapy and free tumor antigen or TDPAs coated AC-NPs. (b) Average tumor growth curves shown in (a). (c) Survival curves of mice in (a) (n=8). Tumor growth over time was compared by two-way analysis of variance (ANOVA) with Bonferroni correction. Data represent mean ± standard error of the mean (SEM). Differences in survival were determined for each group by the Kaplan-Meier method and the overall *P* value was calculated by the log-rank test. *P* value (*, $P<0.05$; **, $P<0.01$; ***, $P<0.005$)